Title:
Biomanufacturing of customized modular scaffolds for critical bone defects

Authours
Bahattin Koc[a,b], Anil A. Acara[a,b], Andrew Weightman[c], Glen Cooper [c], Gordon Blunn[d], Paulo Bartolo[c]
Affiliations
[a] Faculty of Engineering and Natural Sciences, Sabanci University, Orhanli-Tuzla, Istanbul, 34956, Turkey
[b]3D Bioprinting Laboratory, Sabanci University Nanotechnology Research and Application Center, Orhanli-Tuzla, Istanbul, 34956, Turkey
[c] School of Mechanical, Aerospace and Civil Engineering, Manchester Institute of Biotechnology, University of Manchester, Manchester, UK
[d] School of Pharmacy and Biomedical Sciences, University Portsmouth, Portsmouth, UK

Abstract
There is a significant unmet clinical need for modular and customized porous biodegradable constructs (scaffolds) for non-union large bone loss injuries. This paper proposes modelling and biomanufacturing of modular and customizable porous constructs for patient-specific critical bone defects. A computational geometry-based algorithm was developed to model modular porous constructs using a parametric femur model based on the frequency of common injuries. The generated modular constructs are used to generate biomimetic path planning for three-dimensional (3D) printing of modular scaffold pieces. The developed method can be used for regenerating bone tissue for treating non-union large bone defects.

Introduction
Bone has a good healing capacity to regenerate itself for small defects. However, the regeneration potential of the bone is limited for large or critical size defects (1). For critical bone defects, traditional methods such as internal fixation, bone shortening, external fixation and the diamond concept have been used. Internal fixation methods such as intramedullary nails or plates to stabilise bone gaps after septic conditions increase the risk of complications as recurrent infections after internal fixation and may lead to even larger defects (2). Bone shortening with excision of the non-united bone, enables bone healing to begin immediately and assists soft tissue coverage by reducing the defect size or soft tissue tension. In cases where the defect is too large to close immediately, gradual shortening (5 mm per day) may be undertaken. However, for very large bone defects (>8 cm), shortening must be combined with other modes of treatment. External fixation based on the principle that bone and soft tissues can be regenerated under tension applied across a cortectomy, involves the application of a modular-ring external fixator with trans-osseous wires attached to the ring. The main advantage of this technique is that it enables early weight bearing, stimulates local blood flow, produces good quality bone and can be applied to bone defects ranging between 2 to10 cm in size (3). However, it frequently presents complications caused by metal wires transfixing and cutting through soft tissues as the frame is extended to lengthen the bone (4).

The “diamond concept” is based on: osteogenicity (mesenchymal stem cells), osteoconduction (scaffolds), osteoinduction (growth factors), mechanical stability and vascularity. Masquelet (5), explored the concept by proposing a two-stage method. Firstly, a cement spacer is placed in the bone defect, inducing the formation of a biological membrane around it. Secondly, the cement spacer is removed, and bone graft is placed within the tube

of the induced membrane. This membrane is impermeable, hyper-vascular and biologically active. It forms a strong closed biological chamber after the cement removal, maintaining the volume for bone grafting, decreasing resorption of the cancellous bone and preventing ingrowth of soft-tissue. Similar to this method, the use of bone grafts, particularly free vascularised bone grafts that contains an internal vascular network, have been explored to treat bone defects allowing short union times and high union rates (6). These autografts are osteogenic, osteoinductive, osteoconductive and have no risks of immunogenicity and disease transmission (7). However, the main complications are related to pain and morbidity in the donor site, limited quantity and availability, prolonged hospitalization time, the need for general sedation or anaesthesia, risk of deep infection and haematoma, extended non-weight bearing and the risk of inadequate graft hypertrophy.

Recently, biofabrication, the combined use of additive manufacturing techniques, biocompatible and biodegradable materials, cells, growth factors, etc., have been explored to produce bioactive scaffolds (synthetic grafts), as an alternative to biological grafting (8, 9). These scaffolds can be designed to match the defect site, being produced in a controlled and reproducible way using a wide range of polymers, ceramics, and polymer/ceramic mixtures. Several compositions and scaffolds with different topologies and pore sizes were produced and assessed from a mechanical and biological point (10-15), presenting promising results in animal studies (16). Degradation studies and the effect of process conditions on the performance of these scaffolds has also been investigated. To achieve a uniform resorption of the scaffolds, degradation of polymer and ceramic materials must be controlled.

In summary, there is a significant unmet clinical need for a solution for the treatment of large bone loss injuries. We aim to develop a modular and customized porous biodegradable construct (scaffold) for non-union large bone loss injuries. In this paper we present methods for modelling and biomanufacturing of modular and customizable porous constructs for patient-specific critical bone defects. Computational geometry-based algorithms are proposed to model modular porous constructs using a parametric bone model based on the frequency of common injuries. The generated modular constructs are then used to generate biomimetic path planning for three-dimensional (3D) printing of modular scaffold pieces. The developed method can be used for regenerating bone tissue for treating non-union large bone defects.

Materials and Methods

3D Modelling of Customized Modular Scaffold

To be able to create modular porous blocks, the bone defect volume is represented with a set of parametric surfaces, O. Since the modular blocks will be stacked up on an intramedullary implant (i.e., intramedullary femoral nail) as shown in Fig. 1. The radius of this nail changes throughout the bone and defined as R_{nail} . The defect volume O is then segmented based on the similarities between the geometries so similar sections can be combined based on the minimum allowable height and also maximum errors $h_{module,}$ $D_{allowable}$, respectively. Algorithm 1 was developed to take the defect area and segment it to several modular blocks as shown in Fig. 1. These modular blocks can be generated based on the anthropometric data where wide-range of sizes can be created so it can be customized for a specific patient. In Algorithm 1, the object **O** is first sliced to generate contour curves CO_q ; similar curves are then clustered in a set of contours called , m=0, … M and a=0, …, A with the tolerance . To create the most similar and the least number of modules possible, each clustered contour set is replaced with a fit contour, which is represented with $C_{i,}$ i=0,.,I . To create the final 3D geometry of each different module,$M0_q$, q=0, …, MN, each fit contour is extruded along the femoral shaft axis. In the transition zone between two different contours, lofting can be executed using different consecutive fit contours. At the final stage of the

creation of modules, M_q ,q=0,…,MN the intramedullary femoral nail's volume is subtracted from the whole modules.

Algorithm 1: Creation of Scaffold Modules

INPUT: $O, h_{module}, D_{allowable}, R_{nail}$

OUTPUTL: $\{M_q\}_{q=0,\ldots,MN}$

START

Create_Modules() {
C$_m$ ← {} ; a_m ← {} ; CO$_m$ ← {} ; MO$_m$ ← {} ; M$_m$ ← {} /***Initialization***/
CO_q ← Intersect(O, Pl_{XY_q})
While $(i < q)$ {
$j = i + 1, m \leftarrow 0$
While $(j < q)$ {
$k \leftarrow 0$; $a \leftarrow 0$
While $(k < DN)$ {
P_{t_d} ← ClosestPoint($P_{t_{CO_{qk}}}, CO_j$)
D = Distance ($P_{t_d}, P_{t_{CO_{qk}}}$)
If ($D = D_{allowable}$) {
If ($k = DN - 1$) {
$C_{ma} \leftarrow CO_i$; $k = k + 1$; $j = j + 1$; $a = a + 1$
Else
$k = k + 1$ } /*** End of 2nd If statement***/
Else
$k \leftarrow DN$; $k \leftarrow q$
} /*** End of 1st If statement***/
} /*** End of 3rd While statement***/
} /*** End of 2nd While statement***/
$a_m \leftarrow a$; $i = i + a$; $m = m + 1$;
} /*** End of 1st While statement***/
$\forall \boldsymbol{a} \in a_m$
For $(i = 0\ to\ m)$ {
For $(j = 0\ to\ a)$ {
$CO_i \leftarrow C_{ij}$
} /*** End of 2nd For-loop***/
$C_i \leftarrow FitACurve(\ CO_i\ )$
} /*** End of 1st For-loop***/
$CO_q \leftarrow Replace(CO_q, C_m)$
For $(q = 0\ to\ MN)$ {
$MO_q \leftarrow Extrude(CO_q, h_{module})$
$M_q \leftarrow Difference(\ MO_q, R_{nail})$
} /*** End of For-loop***/
END /*** End of Create_Modules( )***/
END

After obtaining the modular blocks, they have to be porous to allow blood to bring necessary nutrition and oxygen to the defect area and also remove the waste material from it. Traditionally, the porous structures also called tissue scaffolds are made with regular porosity by laying opposing struts, i.e., along 0o-90o angles. In this paper, the porosity is designed to change following the bone geometry. Similar to a natural bone itself, the scaffold porosity changes from the middle of the bone to outer bone biomimetically. After the scaffold modules are designed, they need to be biomanufactured using additive manufacturing (three-dimensional, 3D printing) processes. During the printing process, it is important to have a continuous path where the nozzle deposits (extrudes) biomaterial layer by layer with no- or minimum- movements between depositions. Therefore, to have biomimetically vary

porosity and also 3D print modular blocks continuously, a novel continuous path planning algorithm (Algorithm 2) is developed.
First, the generated modular blocks $\{M_q\}_{q=0,\dots,MN}$ sliced based on the layer thickness (nozzle diameter, Dn) and represented as cross-sectional contours. The set of cross-sectional curves are defined as, CO_q^s, q=1 ,…, B.. In the example femur case (Fig. 2), q is given as 2 CO_0^s represents the structure's outer morphological shape at the corresponding layer s, and represents the intramedullary femoral nail's cross-sectional shape at the same layer. Algorithm 2, creates a continuous path planning using these set of cross-sectional curves. First, both curves are divided such that the distances between points are equal to each other. These points are represented with $P_{t_{qi}}^s, i = 0, \dots, DN\text{-}1$, where DN represents the number of points at each contour. The points at each cross-sectional contours are matched by minimizing the distance between them. Here, the intersection between connecting line segments and also between the contours are not allowed to avoid any self-intersections. After the $P_{t_{qi}}^s$ at each contour are matched, they are connected as a continuous zig-zag pattern as shown in Fig. 2. Connecting the set of points in an orderly zig-zag pattern (Fig. 2), zig-zag paths are created and stored in global path planning points $P_{t_d}^s, d = 0, \dots, A.$. After creation of the zig-zag patterned layer, a continuous spiral-like pattern is generated at the consecutive layer. Here, zig-zag patterns are divided by DNL segments. Starting from either outer or inner contour, again a continuous spiral-like pattern is generated at the next consecutive layer. By changing the number of segments at each contour DN and on zig-zag patterns DNL, the desired porosity can be achieved and controlled at each layer as shown in Fig. 2. For 3D printing path planning, a layer with the zig-zag pattern is deposited first, and then the spiral-like path is followed either from the outer or inner contour depending on the last location. After finishing the spiral-like path, again the zig-zag pattern is followed until the whole scaffold module is completed. By adding and connecting zig-zag-like and spiral-like patterns at each layer continuously, a 3D porous network for each modular block can be generated. Fig. 2 shows zig-zag and spiral layers with varying DN and DNL and resulting porosity levels for two different modular blocks. As shown in Fig. 2. by an increasing the number of segments (DN or DNL), the porosity of the whole structure can be changed and controlled. Moreover, the porosity at each layer can be controlled by adjusting the individual parameters at each layer. This way, the porosity and micro-architecture of scaffolds can be controlled based on the mechanical and also biological requirements of the targeted tissue.

Algorithm 2: Continuous Path Planning

INPUT: $D_n, DN, DNL, \{M_q\}_{q=0,\ldots,MN}$

OUTPUTL: $\{P_{t_d}^s\}_{d=1,\ldots,D}$

START

Create_Layers() {
∀ s
For (s=1 to n_l){
  If ($s\ (mod4) = 0$) **Then**
    Create _ZigZag1_Layers ( )
  ElseIf ($s\ (mod4) = 1$)
    Create _Circular1 _Layers ( )
  ElseIf ($s\ (mod4) = 2$)
    Create _ZigZag2_Layers ( )
  ElseIf ($s\ (mod4) = 3$)
    Create _Circular2 _Layers ( )
  } /*** End of If statement***/
} /*** End of For-loop***/
Create _Zigzag1_Layers ( ) {
∀ CO_q^s
$d \leftarrow 0$, $P_{t_d}^s \leftarrow \{\}$ /***Initialization***/
For (i=0 to 2*DN-1){
  If ($i\ (mod4) = 0$) **Then**{
    $P_{t_d}^s \leftarrow P_{t_{0i}}^s$; d= $d+1$
  ElseIf ($i\ (mod4) = 1$) **Then**
    $P_{t_d}^s \leftarrow P_{t_{0(i+1)}}^s$; d= $d+1$
  ElseIf ($i\ (mod4) = 2$) **Then**
    $P_{t_d}^s \leftarrow P_{t_{1(i-1)}}^s$; d= $d+1$
  ElseIf ($i\ (mod4) = 3$) **Then**
    $P_{t_d}^s \leftarrow P_{t_{1(i-1)}}^s$; d= $d+1$
  } /*** End of If statement***/
  Store $P_{t_d}^s$ information in the Script file as tool-path for biodegradable thermoplastic's nozzle over L^s
} /*** End of For-loop***/
$s = s+1$;
END /*** End of Create _Zigzag1_Layers ( )***/
Create _Circular1_Layers ( ) {
∀ CO_q^s
For (i=0 to DN-1){
  l_i^s=Line ($P_{t_{0i}}^s$, $P_{t_{1i}}^s$)
} /*** End of 1st For-loop ***/
For (j=1 to DNL-1){
  $P_{t_d}^s \leftarrow P_{t_{l_{0(j-1)}}}^s$; d= $d+1$
  For (i=0 to DN-1){
    If ($i = DN-1$) **Then**{
      $P_{t_d}^s \leftarrow P_{t_{l_{0j}}}^s$; d= $d+1$
    Else
      $P_{t_d}^s \leftarrow P_{t_{l_{ij}}}^s$; d= $d+1$
  } /*** End of If statement***/
  } /*** End of 2nd For-loop ***/
  } /*** End of 3rd For-loop ***/
Store $P_{t_d}^s$ information in the Script file as tool-path for biodegradable thermoplastic's nozzle over L^s
  $s = s+1$;
END /*** End of Create _Circular1_Layers ( )***/
Create _Zigzag2_Layers ( )
Create _Circular2_Layers ( )
END

Finite Element Analysis of Scaffolds

After the modular scaffolds are manufactured, they are stacked on the intramedullary nail (implant) and allows the bone to regenerate. Here, intramedullary nail takes most of the load and keeps the modular scaffolds in their place until the bone tissue regenerates.

Although the intramedullary femoral nail is the load-bearing, it is crucial for a scaffold module to provide adequate mechanical support during and after implantation. In the literature, the mechanical modulus for hard tissue scaffolds should be in the range of 10-1500 MPa (17).

To understand the designed modular structure' mechanical modulus, a Finite Element Method (FEM) analysis of consecutive and repeated layers was performed for the different porosity levels (M1-A to -I and M2-A to -C) as shown in Fig. 2. As shown in (Fig 3-a), a compression test was carried out for different porosity and different structure modules. Since the modular scaffolds will be biomanufactured using a biopolymer, Polycaprolactone (PCL), the PCL's elastic modulus E=300MPa and the Poisson ratio of 0.3 was used in the analyses (18). Fig 3 shows the obtained result using the developed FEM. The porosity changes depend on the zig-zag pattern and spiral-pattern layer configurations. Different configurations have different mechanical modulus. Keeping the zig-zag pattern at a constant level and increasing the spiral-pattern density (Fig 3-b) decreases the porosity level. Due to the analysis results, this increment increases the mechanical modulus, but after that, the mechanical modulus decreases. On the other hand, keeping the spiral pattern at a constant level and increasing the zig-zag pattern also decreases the porosity level but this decreases the mechanical modulus of modular structures (Fig 3-c). The same result is also obtained for another modular structure (Fig 3-d). Changing the inputs of Algorithm1 and 2 results in different structures, but they will all have an adequate mechanical modulus.

Implementation and Biomanufacturing of Modular Scaffolds for Femur Case

The developed algorithms are implemented using a Computer Aided Design (CAD) software, Rhinoceros 3D, scripting tools. For demonstration purpose, two different scaffold module design (shown in Fig. 2) have been used. For each modular design, porosity levels are changed as shown in Fig. 4. The continuous tool paths were generated and saved as an instruction to control a custom extrusion-based 3D printer. The 3D printer has a heated metal syringe where the polymeric material is loaded and attached to a head controlled in X-Y-Z-axis. By depositing heated material layer by layer in 3D, modular scaffolds blocks are manufactured. For the demonstration, the first two consecutive layers of chosen modular structures with different porosities were additively manufactured with an extrusion-based 3D printer. The extrusion temperature was set at 65°C, and a pneumatic dispensing unit was used to extrude PCL, having 37 kDa molecular weight, with 250 micron nozzle diameter. The printed final structures and their porosities can be seen in Fig 4.

Conclusions

In this paper, a novel method of biomimetic modelling and biomanufacturing of modular and customized scaffold blocks is presented. Computational methods were developed to generate modular blocks where they can be customized for any bone defects. Porous modular blocks were then generated by controlling the porosity mimicking the actual bone micro-architecture. The developed method generates a porous network following the engineered bone geometry. A custom extrusion-based 3D printer was used to additively biomanfacture the designed porous modular blocks using biodegradable polymers. The developed computational method generates a continuous deposition path plan where zig-zag pattern and spiral-like patterns followed at each layer continuously until 3D porous modules are manufactured. The developed computational algorithms and the FEA model allow the user to generate modular scaffold blocks with required mechanical and biological properties. The developed methods can be used to create patient-specific scaffolds using manufactured porous scaffolds modular blocks to treat critical bone defects.

Acknowledgement

This research is supported by the Engineering and Physical Sciences Research Council (EPSRC) of the UK, the Global Challenges Research Fund (GCRF), grant number EP/R015139/1.

References

1. C.R. Perry, Bone repair techniques, bone graft, and bone graft substitutes. Clinical Orthopedics and Related Research. 1999; 71-86.

2. Schulz AO, Gehrmann S, Glombitza M, Kaufman RA, Bostelmann R, Sascha F, Windolf J. (2015) Reconstruction of septic diaphyseal bone defects with the induced membrane technique. *Injury* 46(4):S121-S124.

3. DeCoster TA, Gehlert RJ, Mikola EA. (2004) Management of posttraumatic segmental bone defects. *Journal of the American academy of orthopaedic surgeon*s 12(1):28-38.

4. Papakostidis C, Bhandari M, Giannoudis PV. (2013) Distratcion osteogenesis in the treatment of long bone defects of the lower limbs. *The Bone and Joint Journal* 95B(12)

5. Masquelet AC, Fitoussi F, Begue T, Muller GP (2000) Reconstruction of the long bones by the induced membrane and spongy autograft. *Ann. Chir. Plast. Esthet* 45(3):346-53.

6. Ashman O, Phillips AM (2013) Treatment of non-unions with bone defects: which option and why? *Injury* 44S1:S43-S45

7. Denry I, Kuhn LT (2016) Design and characterization of calcium phosphate ceramic scaffolds for bone tissue engineering. *Dental Materials* 32(1):43-53.

8. Bartolo P, Kruth JP, Silva J, Levy G, Malshe A, Rajurkar K, Mitsuishi M, Ciurana J, Leu M (2012) Biomedical production of implants by additive electro-chemical and physical processes. *CIRP Annals* 61(2):635.

9. Pereira RF, Bartolo P. 3D bioprinting of photocrosslinkable hydrogel constructs (2016) *Applied Polymer Science* 132(48)

10. Domingos M, Intranuovo F, Gloria A, Gristina R, Ambrosio L, Bartolo P, Favia P. (2013) Improved osteoblast cell affinity on plasma-modified 3-D extruded PCL scaffolds. *Acta Biomaterialia* 9(4):5997-6005.

11. Wang W, Caetano G, Ambler WS, Blaker JJ, Frade MA, Mandal P, Diver C, Bartolo P. (2016) Enhancing the Hydrophilicity and Cell Attachment of 3D Printed PCL/Graphene Scaffolds for Bone Tissue Engineering. *Materials* 9(12):992

12. Fiedler T, Videira AC, Bartolo P, Strauch M, Murch GE, Ferreira JMF (2015) On the mechanical properties of PLC–bioactive glass scaffolds fabricated via BioExtrusion. *Materials Science and Engineering.* C. 57:288-293.

13. Vorys GC, Bai H, Chandhanayingyong C, Lee CH, Compton JT, Caldwell JM, Gardner TR, Mao JJ, Lee FY. (2015) Optimal internal fixation of anatomically shaped synthetic bone grafts for massive segmental defects of long bones. *Clinical Biomechanics* 30(10):1114-1118.

14. A.K.M.B. Khoda, I.T. Ozbolat and B. Koc, “Designing Heterogeneous Porous Tissue Scaffolds for Additive Manufacturing Processes”, Computer-Aided Design, 2013, Vol. 45, No: 13.

15. A.K.M.B. Khoda and B. Koc, “Functionally heterogeneous porous scaffold design for tissue engineering”, Computer-Aided Design, 2013, Vol. 45, No: 11, doi:10.1016/j.cad.2013.05.005 (SCI)

16. Caetano G, Violante R, Ana ABS, Murashima AB, Domingos M, Gibson A, Bartolo P, Frade MA. (2016) Cellularized versus decellularized scaffolds for bone regeneration. *Materials Letters* 182:318-322.

17. Goulet, R. W. et al. The relationship between the structural and orthogonal compressive properties of trabecular bone, J. Biomech. 27m 375–389 (1994).

18. Eshraghi S, Das S, 2010, Mechanical and microstructural properties of polycaprolactone scaffolds with one-dimensional, two-dimensional, and three-dimensional orthogonally oriented porous architectures produced by selective laser sintering. Acta biomaterialia.6:2467-76.

Figure legends

Fig. 1. Modular scaffold blocks representing the defect volume

Fig. 2. Continuous path planning and generated porous modules, (P: Porosity)

Fig. 3. Finite-element Analysis (FEA) of generated modular scaffolds

Fig. 4. Biomanufactured modular scaffolds with varying porosity levels

Figure 1

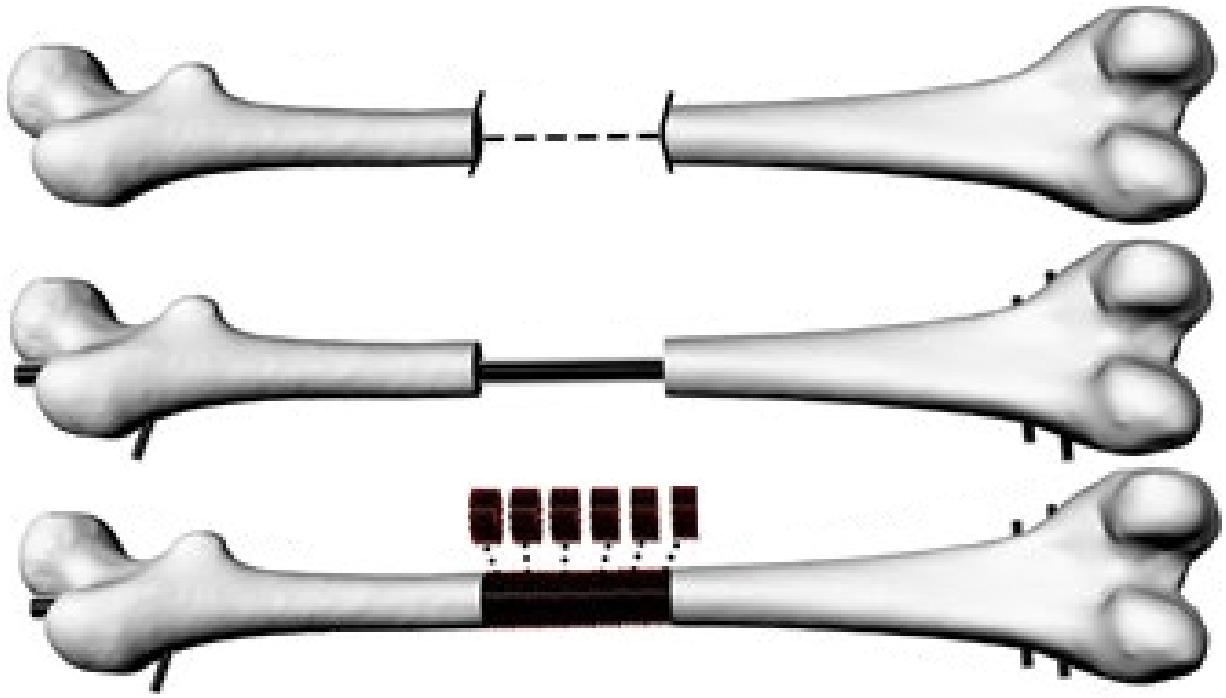

Figure 2

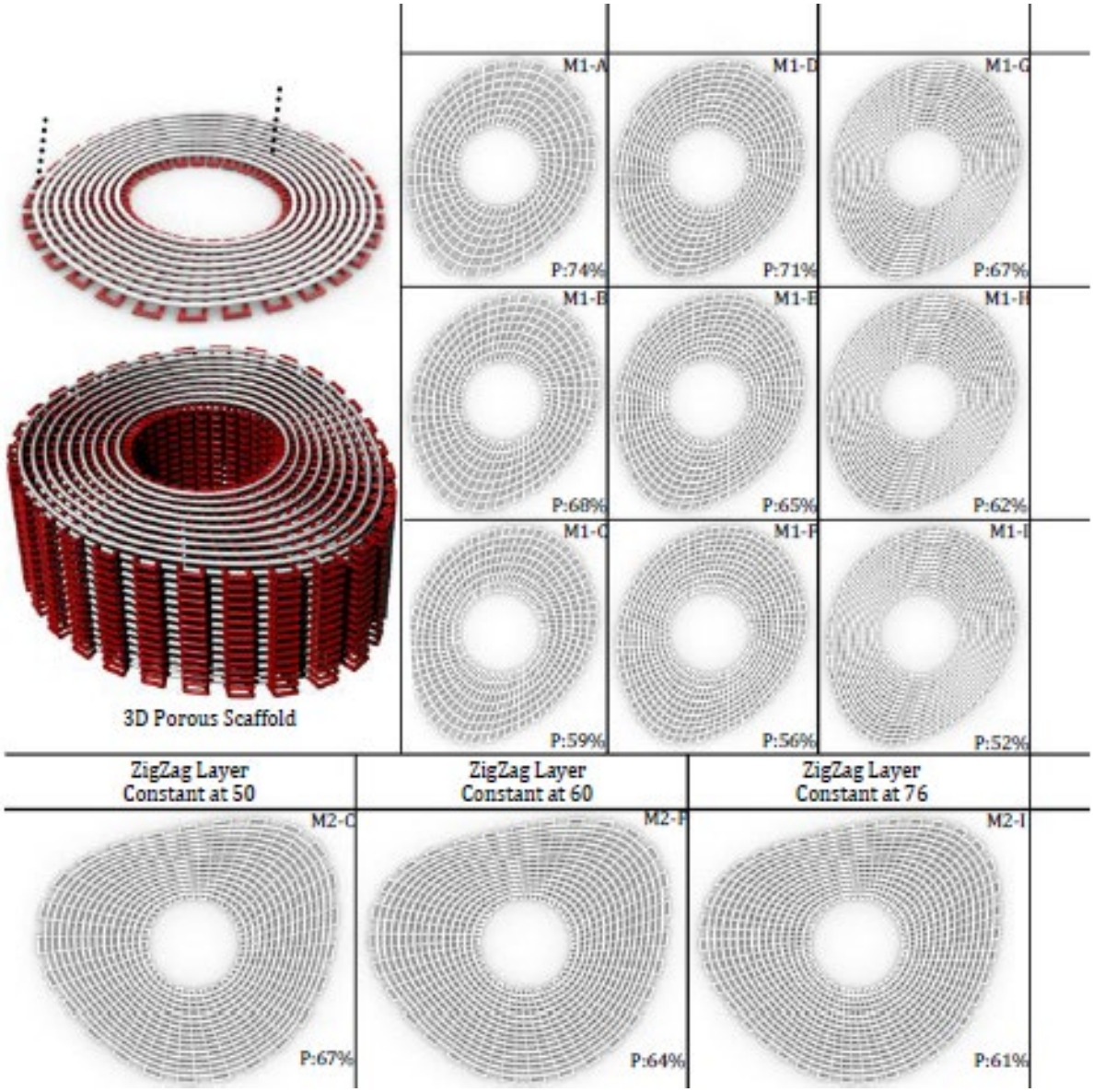
M1-A
P:74%
M1-D
P:71%
M1-G
P:67%
M1-B
P:68%
M1-E
P:65%
M1-H
P:62%
M1-C
P:59%
M1-F
P:56%
M1-I
P:52%
3D Porous Scaffold
ZigZag Layer
Constant at 50
ZigZag Layer
Constant at 60
ZigZag Layer
Constant at 76
M2-C
P:67%
M2-F
P:64%
M2-I
P:61%

Figure 3

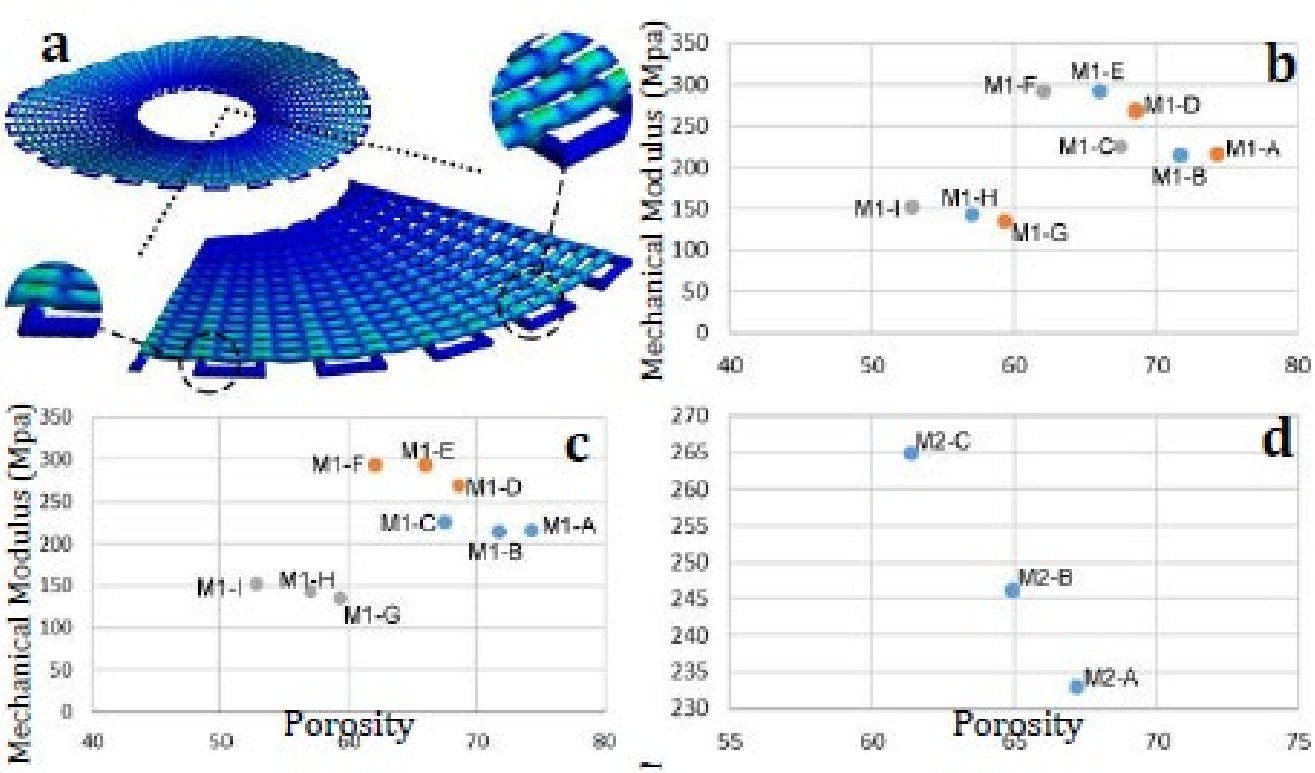
a
b
Mechanical Modulus (Mpa)
M1-F
M1-E
M1-D
M1-C
M1-A
M1-B
M1-I
M1-H
M1-G
c
Porosity
d
M2-C
M2-B
M2-A

Figure 4

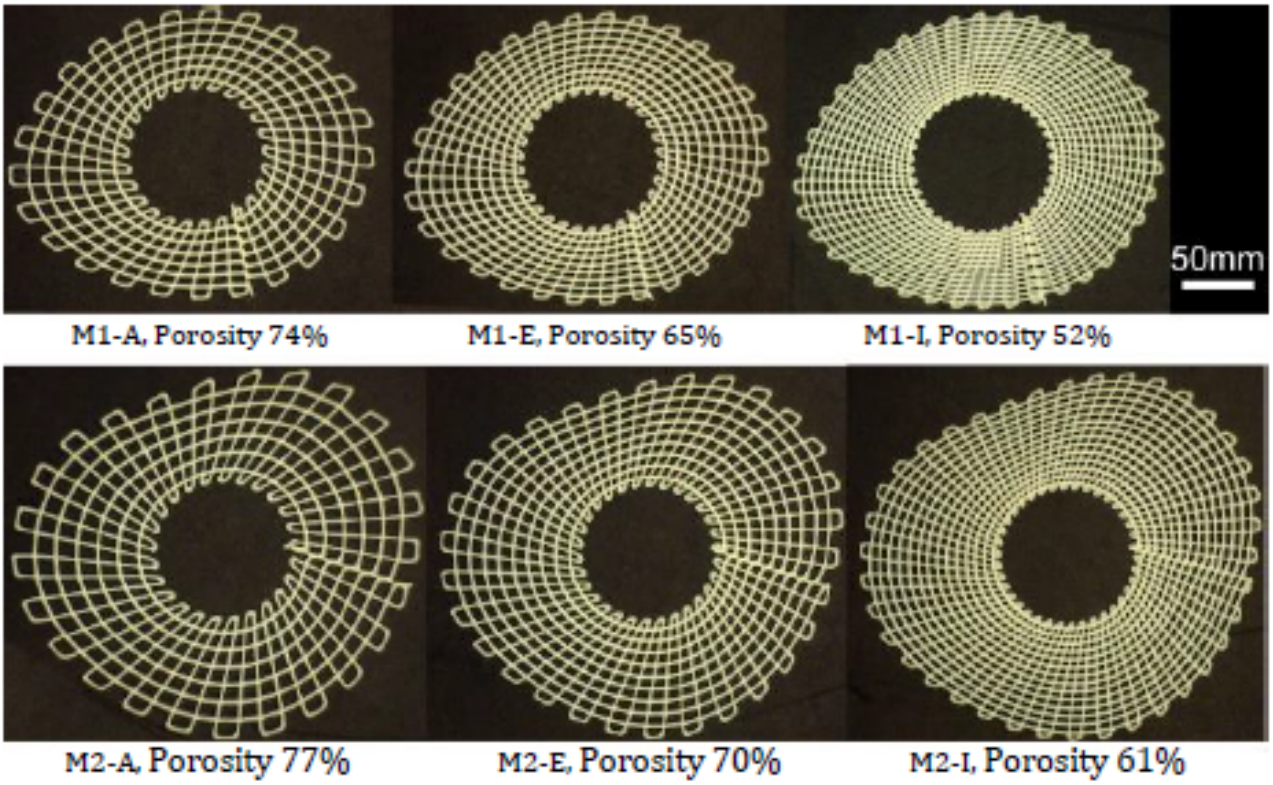
50mm
M1-A, Porosity 74%
M1-E, Porosity 65%
M1-I, Porosity 52%
M2-A, Porosity 77%
M2-E, Porosity 70%
M2-I, Porosity 61%